Düzce University
Journal of Science & Technology

Research Article

Impedance and Interface States Depending on Frequency Analysis of Al/($ZnFe_2O_4$-PVA)/p-Si Structures

Jaafar Abdulkareem Mustafa ALSMAEL [a], Nuray URGUN [b,*], Seçkin ALTINDAL YERİŞKİN [c], Serhat Orkun TAN [d]

[a] *Department of Oil And Gas Engineering, Faculty of Oil and Gas, Basrah University, Basrah, IRAQ*
[b] *Department of Mechatronics Engineering, Faculty of Engineering, Karabük University, Karabük, TURKEY*
[c] *Department of Chemistry And Chemical Processing Technologies, Vocational School Of Technical Sciences, Gazi University, Ankara, TURKEY*
[d] *Department of Electrical and Electronics Engineering, Faculty of Engineering, Karabük University, Karabük, TURKEY*
** Corresponding author's e-mail: nuray1erkutlu@gmail.com*
DOI: 10.29130/dubited.1395252

ABSTRACT

This study investigates the properties of a film made of zinc ferrite ($ZnFe_2O_4$) doped polyvinyl alcohol (PVA). The film is sandwiched between an aluminum (Al) and p-Si semiconductor layers, and electrical measurements are conducted on the structure in a wide scope of frequency besides voltage. The study evaluates the impacts of the $ZnFe_2O_4$-PVA interlayer on surface-states (N_{SS}), and complex-impedance ($Z^* = Z' - jZ''$). A remarkable impact of the values of series resistance (R_S) and the interlayer on the capacitance-voltage (C-V) and conductance-voltage (G/ω-V) data has been observed at moderate and high frequencies. Hence, the C and G/ω versus V qualities were modified at high frequency to eliminate the outcome of R_S. The Hill-Coleman approach was utilized to estimate the values for N_{SS}. Experimental results confirm that both the N_{SS} , R_S and the interlayer in the metal-polymer-semiconductor (MPS) structures are critical factors that significantly alter the electrical and dielectric properties. The analysis of the results obtained from the impedance study showed divergent behavior. It was observed that the impedance values increase in the low frequency, while they diminish in the higher frequencies, as a result of the mutual effect between the interface and the dipole polarization. The study suggests that due to its high dielectric value, the $ZnFe_2O_4$-PVA interlayer may be a better alternative to conventional insulators for charge/energy storage.

Keywords: *Metal-Polymer-Semiconductor, Complex-impedance, Frequency dependence, Series resistance, Interface states.*

Al/($ZnFe_2O_4$-PVA)/P-Si Yapılarda, Empedans ve Arayüz Durumlarının Frekansa Bağlı Analizi

ÖZ

Bu çalışmada çinko ferrit ($ZnFe_2O_4$) katkılı polivinil alkolden (PVA) yapılmış bir filmin özellikleri araştırılmaktadır. Film, alüminyum (Al) ve p-Si yapı arasına sıkıştırılmış olup, yapı üzerinde voltajın yanı sıra geniş bir frekans aralığında elektriksel ölçümler yapılmıştır. Çalışma, $ZnFe_2O_4$-PVA ara katmanının yüzey durumları (N_{SS}) ve kompleks empedans ($Z^* = Z' - jZ''$) üzerine etkilerini değerlendirmektedir. Orta ve yüksek frekanslarda seri direnç (R_S) ve ara katman değerlerinin kapasitans-gerilim (C-V) ve iletkenlik-gerilim (G/ω-V)

Received: 28/11/2023, Revised: 10/12/2023, Accepted: 27/05/2024

özellikleri üzerinde dikkate değer bir etkisi gözlemlenmiştir. Bu nedenle, R_S etkisini ortadan kaldırmak için C-V ve G/ω-V değerleri yüksek frekansta düzenlenmiştir. N_{SS} değerlerini tahmin etmek için Hill-Coleman yaklaşımı kullanıldı. Deneysel sonuçlar hem N_{SS} hem de R_S'in ve metal-polimer-yarı iletken (MPS) yapısındaki ara katmanın, elektriksel ve dielektrik özellikleri önemli ölçüde değiştiren kritik faktörler olduğunu doğrulamaktadır. Empedans çalışmasından elde edilen sonuçların analizi farklı davranışlar gösterdi. Arayüzey ile dipol polarizasyonunun karşılıklı etkisi sonucunda empedans değerlerinin düşük frekansta arttığı, yüksek frekanslarda ise azaldığı gözlenmiştir. Çalışma, yüksek dielektrik değeri nedeniyle $ZnFe_2O_4$-PVA ara katmanının, yük/enerji depolaması için geleneksel yalıtkanlara nazaran daha iyi bir alternatif olabileceğini öne sürmektedir.

Anahtar Kelimeler: *Metal-Polimer-Yarıiletken, Kompleks empedans, Frekans bağımlılığı, Seri direnç, Arayüzey durumları.*

I. INTRODUCTION

The advancement of semiconductor technology in the past decades has greatly impacted various industries, including computing systems, energy, solar cells, and medicine. The increased understanding of the properties of semiconductor materials has led to improved performance of devices and the development of new applications [1]. Metal-semiconductor contacts (MS) play a crucial role in high-frequency applications, particularly those requiring high efficiency and performance [2]. In order to enhance the characteristics of these devices, insulating materials, such as polymers, are often inserted between the metal and the semiconductor [3]. Polymers are attractive materials with their low cost, broad application areas, big surface-to-volume ratio in some forms, and dopant-suitable nature [4]. However, their inability to conduct electricity makes them unsuitable for specific applications in which electrical conductivity matters. Thus, these materials are doped with conductive substances, such as zinc ferrite ($ZnFe_2O_4$), to overcome this limitation [5]. After the usage of a doped interlayer in an MS structure, some abnormal behaviors can be observed in the structures' characteristics. For example, a negative capacitance (NC) peak in the structure's characteristics was observed in an earlier study, which investigated the influence of surface-states (N_{SS}), utilizing the low-high frequency capacitance approach depending on the voltage [6]. For the present study, the impact of N_{SS} was determined according to the (Hill-Coleman) approach, which varies depending on frequency. A compound of zinc, iron, and oxygen known as zinc ferrite is known for having distinct magnetic and electrical properties [7]. It belongs to the spinel family of substances, and its crystal structure is highlighted by cation-occupied tetrahedral and octahedral sites.

Many studies have been carried out in recent years to reveal the electrical, dielectric and impedance properties of structures similar to the structure used in this study. In a study in which an MPS structure was investigated with (Cu_2O–CuO–PVA) inter-layer, the researchers observed wide dispersion on the values in their C-V-f and G/ω-V-f plots especially in the depletion stage due to the distribution and lifetime of *Nss*. Moreover, they related these dispersions also seen in the accumulation due to series-resistance (R_S) and polymer interlayer effects [8]. As a way to comprehend the dielectric behavior of the structure, the impedance results were also analyzed using the equivalent electrical circuit model in another study. Since the researchers related the high dielectric losses with the losses in the energy on the low-frequency scale, they concluded that in low frequencies, grain boundaries, N_{SS} and surface/dipole polarization affect the structure's dielectric response. In contrast, they related this behavior with the grains at high frequencies since there would be less energy necessity for the hopping processes in high frequencies [9]. In another study [10], which revealed the decreasing dielectric losses and easier hopping processes as a result of the high-frequency effect, the researchers found that the (NG:PVP) interlayer had high dielectric values, which shows more charging/energy-storing ability of the device, indicating that organic interlayers can replace conventional insulators. Additionally, several researchers carried out a study of the impedance spectroscopy (IS) method by utilizing appropriate equivalent circuits, which included estimates of the effects of *Nss* and grain boundaries on the conductivity behavior changes [11]. A study group noticed that the device manufacturing process was efficient, with the devices seen to keep 75% of their charge after 1400 seconds. This work provides an

opportunity to use the recently created PVA-PAA-glycerol and a simplified manufacturing method for organic memory device applications based on nanoparticles as charge storage units [12]. The IS analysis has also proven in understanding and improving the performance of the materials, including their usage in alternative ion batteries and catalysis applications [13]. In a recent study, researchers explored how glycerol plasticizers influence the conductivity of Chitosan-derived NCSPEs. The electrical and electrochemical upshots of these nanocomposite films were assessed using AC conductivity and resistivity. The results indicated an improvement in charge transfer resistance with increasing glycerol content, making them candidate materials for EDLC applications [14]. Another study's outcomes revealed the importance of R_S and N_{SS} in the influence of structure properties. The C & G/ω –V plots at high-frequency levels have been improved to remove the *Rs* impact. The outcomes affirmed that ZnS-PVA significantly improved the MPS structure performance in storing electrical charges [15].

In a recent study on the production of Al/ZnO/p-Si (MOS) type Schottky diodes, the usage of ZnO powders produced by biological method as a new approach in this type of semiconductor devices and the effect of graphene oxide (GO) on electrical properties were investigated and the obtained results were compared. As a result, it was observed that the biological method was favorable in the Schottky diode structure and GO doping improved the performance of the device [16]. Similar to this study, by reporting the frequencies feedback of C & G/ω data properties of PVA interlayered Au/n-Si structures, the effects of interface snares and R_S were investigated by impedance computations. In conclusion, it is suggested that PVA interlayer doping with CdTe is a good applicant compared to customary nonconductors, due to its flexibility, higher endurance, facility of growth process, lower price and lower molecular weight [17]. In another study, current-voltage measurements of the Cr/Chlorophyll-a/n-GaP/Ag device fabricated by spin-coating method at 300 °K and electrical parameters were calculated using thermionic emission theory, Norde and Cheung functions. According to the measurement results taken in light and dark environments, it can be considered that the chlorophyll-a layer positively affects the performance of the device. As a result, it is thought that chlorophyll-a layer is photosensitive and will be a new material for use in optoelectronic devices [18]. Revealing that Gr doped in PVA can cause substantial alterations in both dielectric and electrical parameters in MS structures, the researchers noted in their study that, especially interfacial states, series resistance and polarization can change the characteristics of the structure at different voltages. Furthermore, they emphasized that a doping rate of 3% graphene in PVA results in enhanced electrical and dielectric properties [19].

The high magnetic susceptibility of $ZnFe_2O_4$ makes it useful in various applications like microwave devices and magnetic recording media [20]. $ZnFe_2O_4$ also has other probable applications in optical, magnetic, and dielectric materials such as sensors, capacitors, catalysts, etc [21]. Due to its strong chemical stability, $ZnFe_2O_4$ is also resistant to corrosion from acids and bases [22]. Moreover, an earlier study has shown successful outcomes like fine-grained microstructures and superior electromagnetic properties at low cost when used with Ni by the sintering process at low and high temperatures [23]. Another study showed that $ZnFe_2O_4$ has remarkable optical properties in addition to its magnetic and electrical characteristics, with a high transparency ratio of around %85 and wavelength over 550 nm for a fabricated thin film [24]. While doped polymers with zinc ferrite have the potential for a great variety of implementations in the light of the literature, when analyzing this doped polymer in an MS study, the primary factor for the system, in general, is the switching mechanism of the structure. Thus, one of this field's characteristics, which is necessary to investigate, is the complex impedance in a MIS/MPS device since the added layer is expected to change through the entire conduction behavior with small or big degrees. An electrical circuit's resistance to an alternating current is measured by impedance. It is a complex quantity comprising two parts: reactance and resistance. The circuit's impedance is subject to alteration depending on the alternating signal frequency [25]. The opposition to the flow of electrical current through a system is called impedance in the MPS structure. The characteristics of the metal, polymer, and semiconductor materials utilized and the contact between them affect the impedance of an MPS structure.

II. EXPERIMENTAL DETAILS

Al/$ZnFe_2O_4$-PVA/p-Si measurement and manufacture procedures often require many steps. The $ZnFe_2O_4$-PVA composite is made by mixing the nanoparticles with PVA polymer. Then, a solvent is combined with this composite to produce a solution suitable for electro-spinning. The interlayer $ZnFe_2O_4$-PVA is made using the electrospinning process. By drawing the solution via a tiny nozzle with a high voltage, thin fibers are produced, which are then assembled on a grounded collector. Previous works have covered in detail the measurement and manufacturing of the structure as well as the electrospinning approach for fabricating interlayer $ZnFe_2O_4$-PVA [26].

III. RESULTS AND DISCUSSION

Schottky barrier diodes (SBDs) are a type of semiconductor device that utilizes an MS interface to create a rectifying junction. However, it has been shown in the literature that SBDs with a metal-insulator-semiconductor (MIS) or MPS structures exhibit distinct properties compared to MS-type SBDs [27], [28], [29], [30]. The inclusion of an interlayer between metal and semiconductor drastically alters the electrical characteristics of the structure. One example of this can be seen in the case of the Al/($ZnFe_2O_4$-PVA)/p-Si (MPS) structure. The empirical C & G/ω –V data at ordinary room temperature conditions have shown that the structure's C-V tracings exhibit depletion, inversion, and accumulation regions for each frequency.

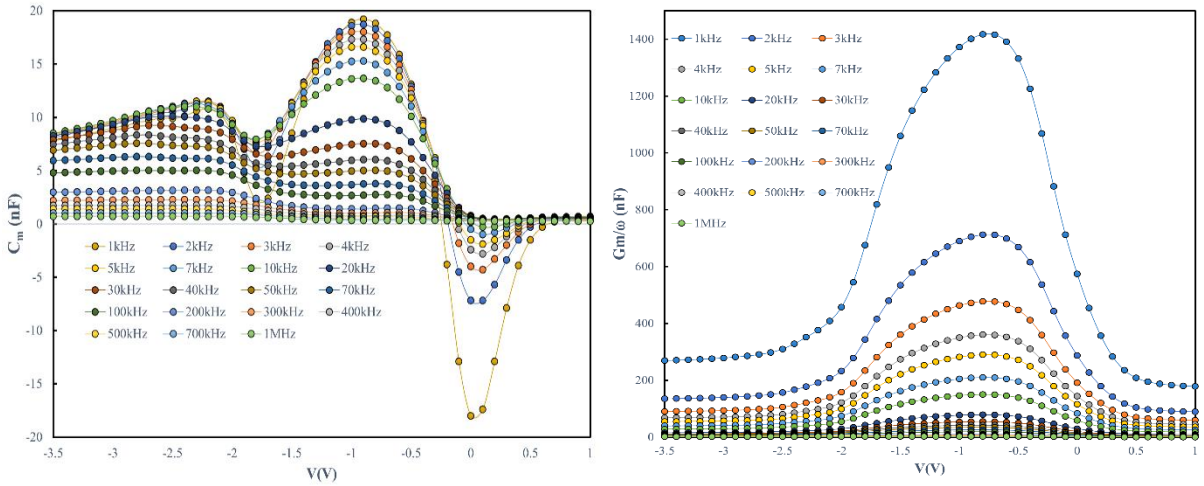

(a) ***(b)***

Figure 1. (a) *Capacitance – Voltage and* ***(b)*** *Conductance – Voltage characteristics of MPS structure.*

In the study, the MPS structure's (*C*-*V*) and (*G*/*ω*-*V*) feature were analyzed at -3,5 V – 1 V voltage interval since this range encompasses the majority of the depletion and accumulation zones, which were observed at this very scale and, significantly impact the MPS structure performance. By focusing on this specific range, it was able to gain more comprehending of how the MPS structure's interface layer affects the device's impedance properties and how it can be optimized for specific applications. The electrical behavior of materials can be investigated using the technique known as complex impedance spectroscopy. It can be utilized to investigate the dielectric characteristics of the interlayer ($ZnFe_2O_4$-PVA) in the context of an MPS structure. Z^* is the abbreviation of the material's complex impedance, as described in the following equation, consists of both a real component (Z') and an imaginary component (Z'') [8]. These components collectively influence the device's response and play a paramount role in shaping the quality of the conducted signal, especially in depletion and accumulation levels. Additionally, they contribute to the energy storage capabilities of the device in inversion and depletion states.

$$Z^* = Z' - j.Z'' \quad (1)$$

where j is the imaginary unit, Z' represents the real term of impedance, and Z'' represents the imaginary term of impedance. When evaluating the electrical behavior of an MPS structure, the measured capacitance (C_m) and conductance (G_m) serve to define its complex impedance (Z^*) through the following equations where ω is the angular frequency [31]:

$$Z' = \frac{G_m}{G_m^2 + (\omega \cdot C_m)^2} \quad (2)$$

$$Z'' = \frac{\omega . C_m}{G_m^2 + (\omega \cdot C_m)^2} \quad (3)$$

Figs 2(a) and (b) chart the complex impedance (Z^*) variation with applied voltage across divergent frequencies. These parameters show that the real component Z' decreases with increasing frequency, while it can be seen different patterns of change between the increase and decrease in Z'' values with the change in frequency. A severe drop in both components of impedance values can be observed within a certain voltage range, (-1) - (0) volts. This reduction becomes less noticeable as the voltage increases in the reverse and forward directions. As the frequency increased, the Z' values decreased; Conversely, Z'' values increased, as shown in Fig 3. The presence of fixed charges and N_{SS} through the MPS interface accounts for this behavior. So, the N_{SS}-induced imperfections may cause bandgap formation at the semiconductor and metal interface. Besides, at a voltage of 0.2 volts, it becomes evident that NC values correspond to negative Z'' values. This correlation can also be observed at this specific voltage point. It arises due to the occurrence of N_{SS} in the semiconducting layer through the MS interface. The NC is an effective instrument for inter-layered MS structures as it can be used in the design of high-frequency devices such as oscillators and amplifiers by means of a device capacitance limiting feature. The researchers have mostly observed NC behavior at low-frequency and forward bias scales, as well as appeared in our study, parallel to the literature, but it can be seen other than these working scales, too [32]. The general acceptance is that NC is an inductive reflectance of the structure's response against to the AC signal, related to the lifetime, N_{SS}, and the minority carrier injection [33], [34].

The two upside elbows at the corresponding positive capacitance values at reverse polarization and one downside elbow at the negative capacitance values at around 0 V in positive polarization in Fig 1(a) are the noticeable results of the material's relaxation in the applied external electrical field due to the lifetime and the excessive capacitance appearance due to the doped materials relative permittivity's change affecting the whole structure's response, respectively. Also, another reason for the reduced effective capacitance is not only because of the entire interlayer's effect of the doped-PVA but also because of the extra capacitive formations due to the surface charges' self-storage/charge effect at low frequencies. Furthermore, these kinds of NC appearances in a doped-interlayered heterostructure's plots show that the NC does not appear only on the directly ferroelectric materials but also on the layered materials with effects of impurities in turn due to the created short-term virtual polarization.

The amplitude of impedance and the phase angle ($\theta°$) between Z' and Z'' can be calculated as by the following expressions:

$$[Z] = \sqrt{Z'^2 + Z''^2} \quad (4)$$

$$\theta = tan^{-1}\left(\frac{z''}{z'}\right) \quad (5)$$

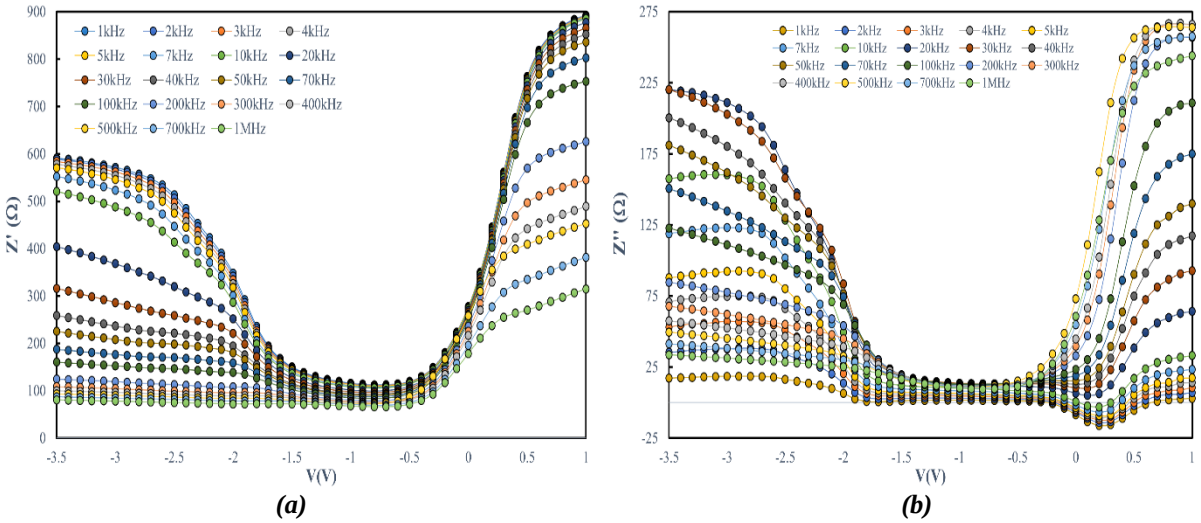

Figure 2. (a) *Z'-V,* ***(b)*** *Z''-V characteristics of MPS structure for different frequencies.*

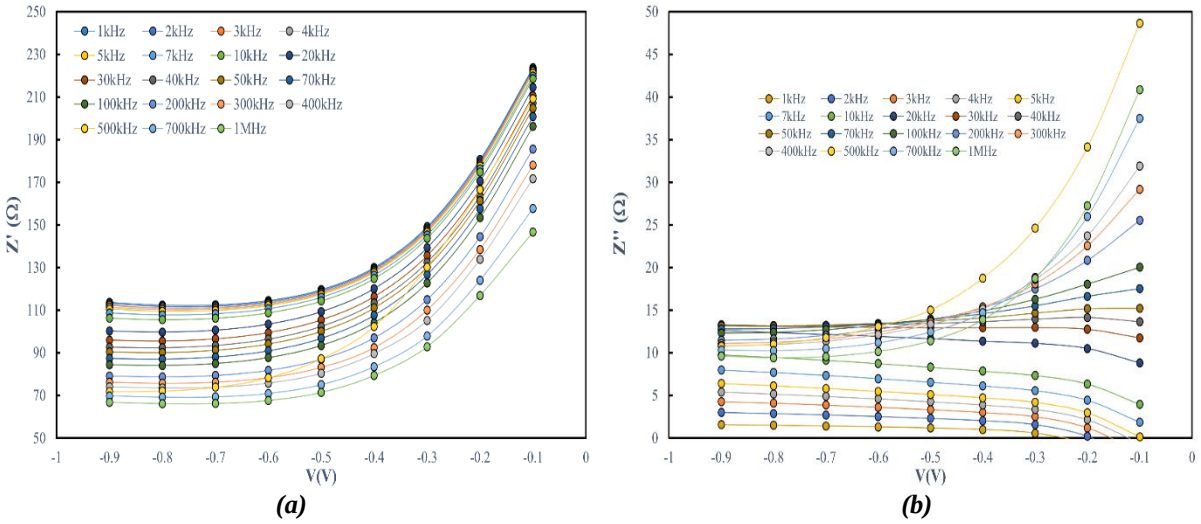

Figure 3. (a) *Z'-V,* ***(b)*** *Z''-V characteristics of MPS structure for different frequencies at voltage range (-1-0).*

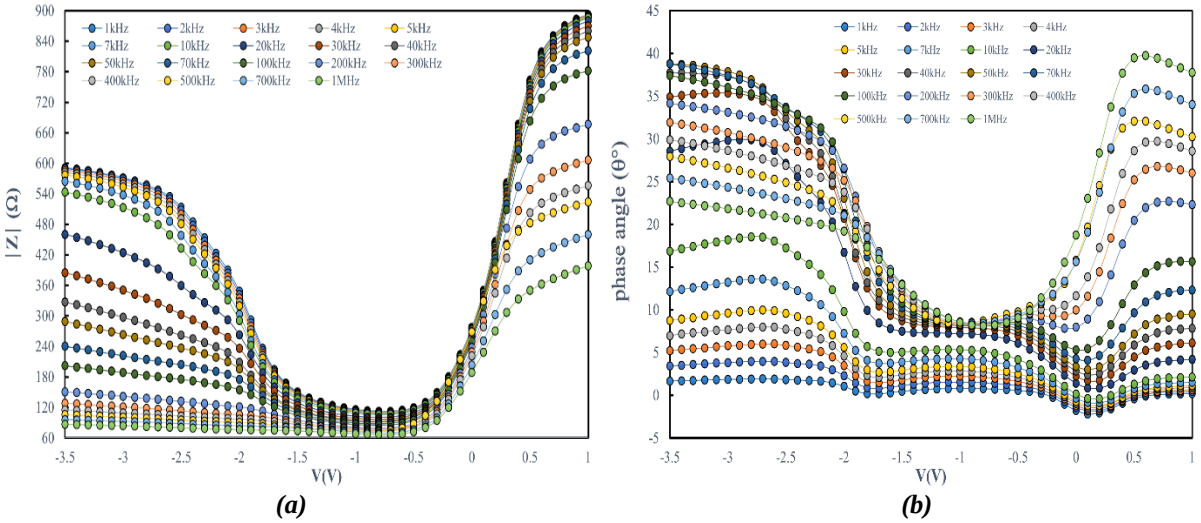

Figure 4. (a) *|Z|-V, (b) Phase angle (θ°)-V characteristics of MPS structure for different frequencies.*

The evolution of the amplitude and phase angle were illustrated in response to biases at different frequencies in Figs 4(a) and (b). Notably, the impedance magnitude exhibits behavior closely mirroring the real and imaginary impedance components, owing to the presence of a low phase angle value ($\theta < 40°$). Moreover, the phase angle attains its minimum while the frequency diminishes. When looking at details in Fig 4(b), the medium, high, and low frequency peaks are located at the beginning, respectively. However, they change their locations specifically after -0,6 V, which can also be observed in the secondary highest peaks in Fig 5. After this bias point, they divide into rising high frequency peaks and lessening medium and low peaks. This division is also observable at the bias point after -0,4 V in Z"-V plot in Fig 3(b). This early appearance of peak division in phase angle, compared to the appearance in the imaginary part of impedance, is due to the *Rs* effects on the conduction, corresponding to after -1 V in Fig 1(a) and after -0,8V in Fig 1(b).

To evaluate the effect of R_S on (C-V) and (G/ω-V) data, these data were corrected at 500 kHz under all biases. The corrected capacitance (C_C) and conductance (G_C) values were acquired through the following equations [35], [36]:

$$C_c = \frac{[G_m^2 + (\omega C_m)^2]C_m}{a^2 + (\omega C_m)^2} \tag{6}$$

$$G_c = \frac{[G_m^2 + (\omega C_m)^2]a}{a^2 + (\omega C_m)^2} \tag{7}$$

Where a is equivalent to the equation.

$$a = G_m - [G_m^2 + (\omega C_m)^2]R_s \tag{8}$$

These equations take into account the influence of *Rs* on the measured capacitance and conductance values and provide a more accurate representation of the true capacitance and conductance of the MPS structure. By analyzing the corrected values of C_C and G_C, it is possible to obtain a better comprehension of the electrical properties of the structure and how they are affected by the presence of R_S. The measuring frequency, temperature, and bias conditions can significantly impact the measurement results and the R_S. Therefore, when measuring and correcting the C-V and G/ω-V readings, it is vital to take these parameters into account in order to achieve accurate findings.

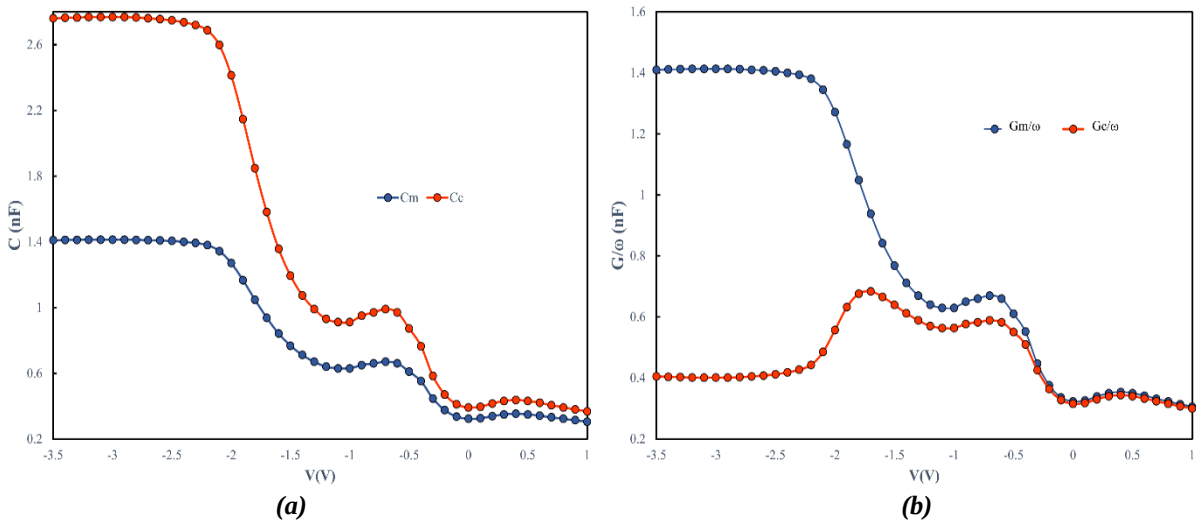

Figure 5. (a) *C_C-V, C_m-V, and* ***(b)*** *G_C/ω-V, C_m-V characteristics for MPS structure.*

Thus, the C-V and G/ω-V data are presented in Figs 5 (a) and (b), correspondingly, before and after correction. When the C-V characteristic is corrected, as shown in Fig 4(a), the increment at C_C values

realizes as the applied biases increase, particularly in the accumulation and depletion zones. Corrected *C* values accurately describe the actual *C* of the MPS structure. However, the corrected conductance (G_C/ω-V) characteristic shows a peak in the depletion zone, demonstrating the possibility of charge transfer over the interface. It is obvious that the values of R_S are important, particularly in the zones of accumulation and depletion. This is due to the fact that the majority of charge transfer occurs in the depletion and accumulation zones. Therefore, when inferring the frequency- and voltage-dependent electrical attributes of the MPS structure, the R_S value should be considered. N_{SS} of MPS can also be determined using the Hill-Coleman approach by following equation [37]:

$$N_{ss} = \frac{2}{qA}\left[\frac{(G_m / \omega)_{max}}{((G_m / \omega)_{max}/C_i)^2 + (1 - C_m/C_i)^2}\right] \quad (9)$$

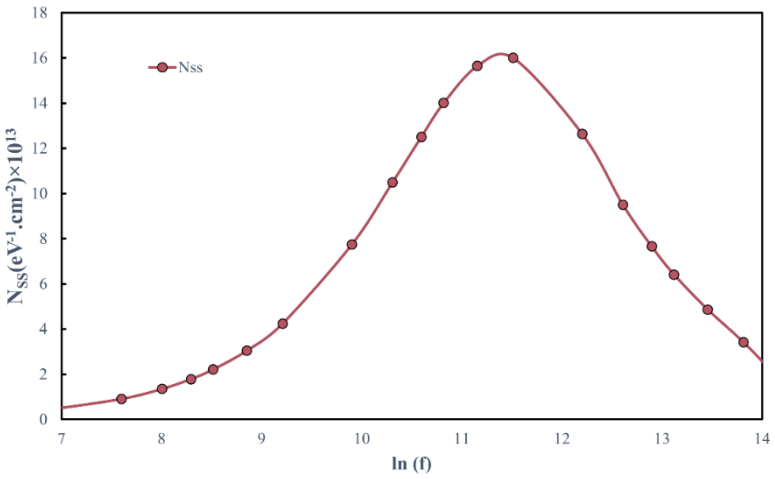

Figure 6. *N_{SS} -ln(f) characteristics for MPS structure.*

The rectifier contacts area (A), measured capacitance (C_m), and conductance (G_m/ω), as well as the interlayer capacitance (C_i), can be used to compute the N_{SS}. The C-V and G/ω-V data in the strong accumulation zone at high frequency (1 MHz) can be used to determine the C_i value [35].

$$C_i = C_{ma}\left[1 + \frac{G_{ma}^2}{(\omega C_{ma})^2}\right] \quad (10)$$

In Eq. 10; the measured values, G_{ma} and C_{ma}, represent the conductance and capacitance at strong accumulation stage, correspondingly. Moreover, Fig 5 pictures each frequency's N_{SS} values derived from equation (9). The values of N_{SS} decline by frequency rising, as seen in Fig 6. This is due to the fact that the N_{SS} are incapable of capturing the AC signal at sufficiently higher frequencies and are not participating in the values of capacitance and conductance. It is critical to mention that this approach is solely applicable when the series resistance is negligible at high frequency and the frequency is high enough to avoid the effect of the depletion region. The Hill-Coleman approach is one of the widely used approach to determine the N_{SS}, however it is also a rough approximation and is only valid for low frequency and low temperature measurements.

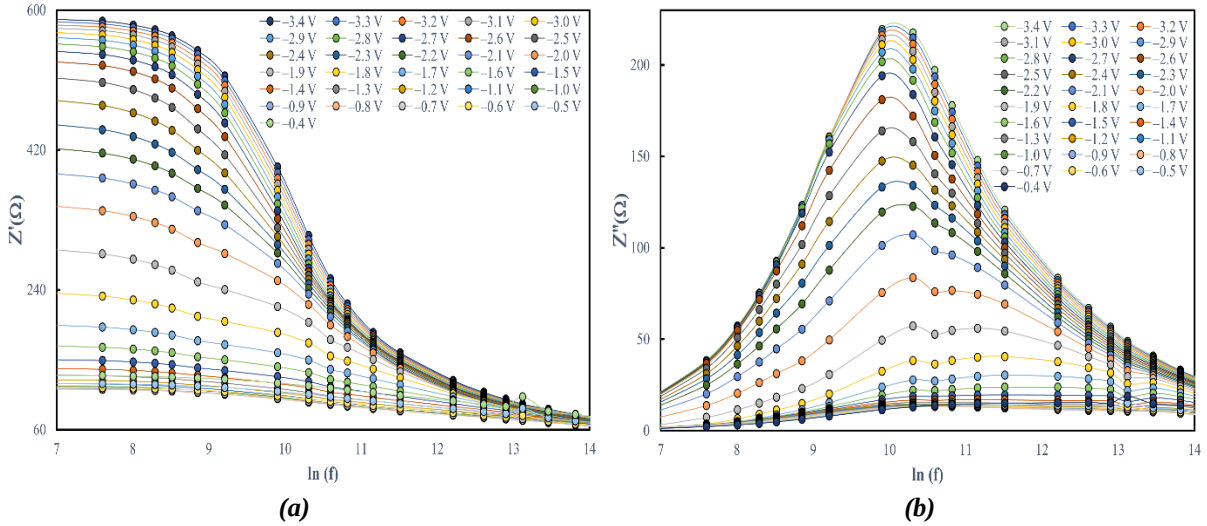

(a) ***(b)***

Figure 7. (a) *Z'-ln(f),* ***(b)*** *Z''-ln(f), characteristics of the structure.*

As shown in Figs 7 (a) and 7 (b), the variations of Z' and Z'' values resulting in distinct outputs of Z^* can be effective at the choice of diverging applications due to the preferred conditions specifically for the voltage range when employed for corresponding negative capacitance scale as in Fig 1 to favor from expected to be decreased power consumption. It is clearly seen in Figure 7 (a) that Z'' values decline in each component of the voltage spectrum with frequency increment. It is also ascertained in Figure 7 (b) that Z'' values are highly frequency dependent and affected by the biases. Z'' values incline with increasing frequency until the highest peak around ln(f)=10.3 Hz after which they start to decline with further increment in frequency.

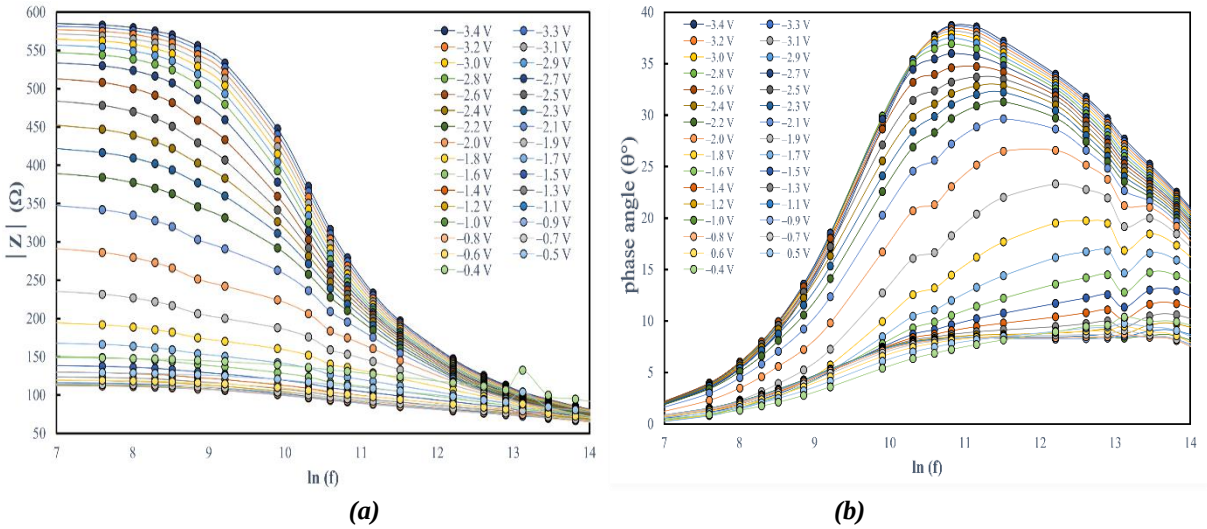

(a) ***(b)***

Figure 8. (a) *$|Z|$-ln(f),* ***(b)*** *Phase angle ($\theta°$)-ln(f) characteristics of MPS structure for different voltage.*

This pattern is also observable for $|Z|$ and the phase angle between both elements of Z^*, as shown in Figs 8 (a) and (b). These trends in values can considerably affect how well the related whole system or device works; therefore, they should be cautiously weighed in the envisagement and execution stages.

IV. CONCLUSION

In the presented paper, the reliance of various impedance properties of Al/($ZnFe_2O_4$-PVA)/p-Si device due to the frequency and polarization have been thoroughly examined. In addition, the frequency-dependent impedance characteristics were inferred by analyzing *C* and *G* data. All these parameters were clearly dictated by both frequency and voltage, particularly for low-intermediate frequencies in the inversion and accumulation zones. The presence of N_{SS} (non-equilibrium charge carriers), their relaxation times, and surface and dipole polarizations were identified as the main reasons behind this frequency and voltage reliance. Furthermore, the real part of impedance was observed to impact the *C* and *G* significantly at high frequencies. The *C* and G/ω data were corrected for high-frequency values in order to take this impact into consideration. The study emphasizes how crucial N_{SS} is as a factor that notably affects the electrical properties of Al/($ZnFe_2O_4$-PVA)/p-Si structures. According to impedance analysis, the majority of the parameters are impacted by variations in the N_{SS}, and this causes a peak in their values at 30 kHz. This understanding of the dielectric properties of this type of structure can be useful in the design and optimization of high-capability electronic devices besides energy storage solutions.

ACKNOWLEDGEMENTS: No funding was used in this study.

ACKNOWLEDGEMENTS: This manuscript was prepared from the results of a published PHD dissertation thesis, which is available at http://acikerisim.karabuk.edu.tr:8080/xmlui/handle/123456789/2682

V. REFERENCES

[1] K. Akarvardar and H.-S. P. Wong, "Technology Prospects for Data-Intensive Computing," *Proc. IEEE*, vol. 111, no. 1, pp. 92–112, 2023, doi: 10.1109/jproc.2022.3218057.

[2] B. L. Sharma, "*Metal-semiconductor Schottky barrier junctions and their applications*," Springer Science & Business Media, NY, 2013.

[3] S. Alptekin, S. O. Tan, and Ş. Altındal, "Determination of Surface States Energy Density Distributions and Relaxation Times for a Metal-Polymer-Semiconductor Structure," *IEEE Trans. Nanotechnol.*, vol. 18, pp. 1196–1199, 2019, doi: 10.1109/TNANO.2019.2952081.

[4] Ş. Altındal, T. Tunç, H. Tecimer, and İ. Yücedağ, "Electrical and photovoltaic properties of Au/(Ni, Zn)-doped PVA/n-Si structures in dark and under 250W illumination level," *Mater. Sci. Semicond. Process.*, vol. 28, pp. 48–53, 2014, doi: 10.1016/j.mssp.2014.05.007.

[5] S. O. Tan, "Comparison of Graphene and Zinc Dopant Materials for Organic Polymer Interfacial Layer Between Metal Semiconductor Structure," *IEEE Trans. Electron Devices*, vol. 64, no. 12, pp. 5121–5127, 2017, doi: 10.1109/TED.2017.2766289.

[6] J. A. M. Alsmael, N. Urgun, S. O. Tan, and H. Tecimer "Effectuality of the Frequency Levels on the C&G/ω–V Data of the Polymer Interlayered Metal-Semiconductor Structure," *Gazi Univ. J. Sci. Part A: Eng. Innov.*, vol. 9, no. 4, pp. 554–561, 2022, doi: 10.54287/gujsa.1206332.

[7] A. Pradeep, P. Priyadharsini, and G. Chandrasekaran, "Structural, magnetic and electrical properties of nanocrystalline zinc ferrite," *J. Alloys Compd.*, vol. 509, no. 9, pp. 3917–3923, 2011, doi: 10.1016/j.jallcom.2010.12.168.

[8] A. Buyukbas-Uluşan, S. A. Yerişkin, A. Tataroğlu, M. Balbaşı, and Y. A. Kalandaragh, "Electrical and impedance properties of MPS structure based on (Cu_2O–CuO–PVA) interfacial layer,"

J. Mater. Sci.: Mater. Electron., vol. 29, no. 10, pp. 8234–8243, 2018, doi: 10.1007/s10854-018-8830-9.

[9] Ç. Oruç, A. Erkol, and A. Altındal, "Characterization of metal (Ag,Au)/phthalocyanine thin film/semiconductor structures by impedance spectroscopy technique," *Thin Solid Films*, vol. 636, pp. 765–772, 2017, doi: 10.1016/j.tsf.2017.03.058.

[10] A. M. Akbaş, A. Tataroğlu, Ş. Altındal, and Y. Azizian-Kalandaragh, "Frequency dependence of the dielectric properties of Au/(NG:PVP)/n-Si structures," *J. Mater. Sci.: Mater. Electron.*, vol. 32, no. 6, pp. 7657–7670, 2021, doi: 10.1007/s10854-021-05482-9.

[11] A. Ashery, M. M. M. Elnasharty, M. A. Salem, and A. E. H. Gaballah, "Synthesis, characterization, and electrical properties of $CuInGaSe_2/SiO_2$/n-Si structure," *Opt. Quantum Electron.*, vol. 53, no. 10, pp. 1–22, 2021, doi: 10.1007/s11082-021-03196-0.

[12] M. Y. Haik, A. I. Ayesh, T. Abdulrehman, and Y. Haik, "Novel organic memory devices using Au–Pt–Ag nanoparticles as charge storage elements," *Mater. Lett.*, vol. 124, pp. 67–72, 2014, doi: 10.1016/j.matlet.2014.03.070.

[13] A. R. C. Bredar, A. L. Chown, A. R. Burton, and B. H. Farnum, "Electrochemical Impedance Spectroscopy of Metal Oxide Electrodes for Energy Applications," *ACS Appl. Energy Mater.*, vol. 3, no. 1, pp. 66–98, 2020, doi: 10.1021/acsaem.9b01965.

[14] J. M. Hadi et al., "Electrical, dielectric property and electrochemical performances of plasticized silver ion-conducting chitosan-based polymer nanocomposites," *Membranes*, vol. 10, no. 7, p. 151, 2020, doi: 10.3390/membranes10070151.

[15] N. Baraz *et al.*, "Electric and Dielectric Properties of Au/ZnS-PVA/n-Si (MPS) Structures in the Frequency Range of 10–200 kHz," *J. Electron. Mater.*, vol. 46, no. 7, pp. 4276–4286, 2017, doi: 10.1007/s11664-017-5363-6.

[16] M. Kırkbınar and F. Çalışkan, "Biyolojik Yöntem ile GO Katkılı Al/(Biyo-ZnO)/pSi Schottky Diyotların Üretimi ve Elektriksel Karakterizasyonu", *DÜBİTED*, vol. 11, no. 3, pp. 1623–1634, 2023, doi: 10.29130/dubited.1171313.

[17] Ç. Ş. Güçlü, Ş. Altındal, and E. E. Tanrikulu, "Voltage and frequency reliant interface traps and their lifetimes of the MPS structures interlayered with CdTe:PVA via the admittance method," *Physica B Condens. Matter*, vol. 677, p. 415703, 2024, doi: 10.1016/j.physb.2024.415703.

[18] F. Ş. Kaya, "Cr/Klorofil-a/n-GaP/Ag Aygıtının Akım-Gerilim Karakteristiklerinin İncelenmesi", *DUBİTED*, vol. 11, no. 4, pp. 1996–2005, 2023, doi: 10.29130/dubited.1271979.

[19] M. Yürekli, A. F. Özdemir, and Ş. Altındal, "Investigation of dielectric and electric modulus properties of Al/p-Si structures with pure, 3%, and 5% (graphene:PVA) by impedance spectroscopy, " *J. Mater Sci.: Mater. Electron.*, vol 35, no. 6, p. 422, 2024, doi: 10.1007/s10854-024-12077-7.

[20] Y. Yang *et al.*, "Synthesis of nonstoichiometric zinc ferrite nanoparticles with extraordinary room temperature magnetism and their diverse applications," *J. Mater. Chem.*, vol. 1, no. 16, pp. 2875–2885, 2013, doi: 10.1039/C3TC00790A.

[21] M. F. Hossain, T. C. Paul, M. N. I. Khan, S. Islam, and P. Bala, "Magnetic and dielectric properties of $ZnFe_2O_4$/nanoclay composites synthesized via sol-gel autocombustion," *Mater. Chem. Phys.*, vol. 271, p. 124914, 2021, doi: 10.1016/j.matchemphys.2021.124914.

[22] G. Fan, Z. Gu, L. Yang, and F. Li, "Nanocrystalline zinc ferrite photocatalysts formed using the colloid mill and hydrothermal technique," *Chem. Eng. J.*, vol. 155, no. 1, pp. 534–541, 2009, doi: 10.1016/j.cej.2009.08.008.

[23] S. Zahi, “Nickel–zinc ferrite fabricated by sol–gel route and application in high-temperature superconducting magnetic energy storage for voltage sag solving,” *Mater. Des.*, vol. 31, no. 4, pp. 1848–1853, 2010, doi: 10.1016/j.matdes.2009.11.004.

[24] M. Sultan and R. Singh, “Magnetic and optical properties of rf-sputtered zinc ferrite thin films,” *J. Appl. Phys.*, vol. 105, no. 7, p. 07A512, 2009, doi: 10.1063/1.3072381.

[25] R. Schmidt, P. Mayrhofer, U. Schmid, and A. Bittner, “Impedance spectroscopy of Al/AlN/n-Si metal-insulator-semiconductor (MIS) structures,” *J. Appl. Phys.*, vol. 125, no. 8, p. 84501, 2019, doi: 10.1063/1.5050181.

[26] J. A. M. Alsmael, S. O. Tan, H. U. Tecimer, Ş. Altındal, and Y. A. Kalandaragh, “The Impact of Dopant on the Dielectric Properties of Metal-Semiconductor With $ZnFe_2O_4$ Doped Organic Polymer Nanocomposites Interlayer,” *IEEE Trans. Nanotechnol.*, vol. 21, pp. 528–533, 2022, doi: 10.1109/TNANO.2022.3207900.

[27] H. Kanbur, Ş. Altındal, and A. Tataroğlu, “The effect of interface states, excess capacitance and series resistance in the Al/SiO_2/p-Si Schottky diodes,” *Appl. Surf. Sci.*, vol. 252, no. 5, pp. 1732–1738, 2005, doi: 10.1016/j.apsusc.2005.03.122.

[28] H.-K. Lee, I. Jyothi, V. Janardhanam, K-H. Shim, H-J. Yun, S-N. Lee, H. Hong, J-C. Jeong, and C-J. Choi, “Effects of Ta-oxide interlayer on the Schottky barrier parameters of Ni/n-type Ge Schottky barrier diode,” *Microelectron. Eng.*, vol. 163, pp. 26–31, 2016, doi: 10.1016/j.mee.2016.06.006.

[29] Ş. Altındal, A. Tataroğlu, and İ. Dökme, “Density of interface states, excess capacitance and series resistance in the metal–insulator–semiconductor (MIS) solar cells,” *Sol. Energy Mater. Sol. Cells*, vol. 85, no. 3, pp. 345–358, 2005, doi: 10.1016/j.solmat.2004.05.004.

[30] D. Ata, S. Altındal Yeriskin, A. Tataroğlu, and M. Balbasi, “Analysis of admittance measurements of Al/Gr-PVA/p-Si (MPS) structure,” *J. Phys. Chem. Solids*, vol. 169, p. 110861, 2022, doi: 10.1016/j.jpcs.2022.110861.

[31] M. Sharma, S. K. Tripathi, “Frequency and voltage dependence of admittance characteristics of Al/Al_2O_3/PVA:n-ZnSe Schottky barrier diodes,” *Mater. Sci. in Semicond. Process.*, vol. 41 pp. 155-161, 2016, doi: 10.1016/j.mssp.2015.07.028.

[32] Z. Berktas, E. Orhan, M. Ulusoy, M. Yildiz, and S. Altındal, “Negative capacitance behavior at low frequencies of nitrogen-doped polyethylenimine-functionalized graphene quantum dots-based Structure,” *ACS Appl. Electron. Mater.*, vol. 5, no. 3, pp. 1804–1811, 2023, doi: 10.1021/acsaelm.3c00011.

[33] E. E. Tanrıkulu, S. Demirezen, Ş. Altındal, and İ. Uslu, “On the anomalous peak and negative capacitance in the capacitance–voltage (C–V) plots of Al/(% 7 Zn-PVA)/p-Si (MPS) structure,” *J. Mater. Sci.: Mater. Electron.*, vol. 29, no. 4, pp. 2890–2898, 2018, doi: 10.1007/s10854-017-8219-1.

[34] S. Demirezen, E. E. Tanrıkulu, and Altındal, “The study on negative dielectric properties of Al/PVA (Zn-doped)/p-Si (MPS) capacitors,” *Indian J. Phys.*, vol.93, no. 6, pp. 739–747, 2019, doi: 10.1007/s12648-018-1355-5.

[35] E. H. Nicollian and J. R. Brews, *MOS (Metal Oxide Semiconductor) Physics and Technology*. John Wiley & Sons, 2002.

[36] H. Tecimer, H. Uslu, Z. A. Alahmed, F. Yakuphanoğlu, and S. Altindal, “On the frequency and voltage dependence of admittance characteristics of Al/PTCDA/P-Si (MPS) type Schottky barrier

diodes (SBDs)," *Compos. Part B Eng.*, vol. 57, pp. 25–30, 2014, doi: 10.1016/j.compositesb.2013.09.040.

[37] W. A. Hill and C. C. Coleman, "A single-frequency approximation for interface-state density determination," *Solid. State. Electron.*, vol. 23, no. 9, pp. 987–993, 1980, doi: 10.1016/0038-1101(80)90064-7.